Access to this work was provided by the University of Maryland, Baltimore County (UMBC) ScholarWorks@UMBC digital repository on the Maryland Shared Open Access (MD-SOAR) platform.

Please provide feedback

Please support the ScholarWorks@UMBC repository by emailing scholarworks-group@umbc.edu and telling us what having access to this work means to you and why it's important to you. Thank you.

Geophysical Research Letters®

Key Points:

- Wildfire aerosols appear to repartition stratospheric chlorine over a 7-month period, with the greatest effect where nights are longest
- Simulations show that observed chlorine repartitioning is inconsistent with chemistry on sulfuric acid/water aerosols
- Long-lived trace gases show that most of the observed midlatitude O_3 decrease after April is explained by transport

Supporting Information:

Supporting Information may be found in the online version of this article.

Correspondence to:

S. E. Strahan,
susan.e.strahan@nasa.gov

Unexpected Repartitioning of Stratospheric Inorganic Chlorine After the 2020 Australian Wildfires

Susan E. Strahan[1,2] , Dan Smale[3] , Susan Solomon[4] , Ghassan Taha[1,5], Megan R. Damon[1,6], Stephen D. Steenrod[1,2], Nicholas Jones[7] , Ben Liley[3] , Richard Querel[3] , and John Robinson[3]

[1]NASA Goddard Space Flight Center, Greenbelt, MD, USA, [2]GESTAR II, University of Maryland Baltimore County, Baltimore, MD, USA, [3]National Institute of Water & Atmospheric Research (NIWA), Lauder, New Zealand, [4]Department of Earth, Atmospheric, and Planetary Sciences, MIT, Cambridge, MA, USA, [5]GESTAR II, Morgan State University, Baltimore, MD, USA, [6]Science Systems and Applications, Inc., Lanham, MD, USA, [7]School of Physics, Wollongong University, Wollongong, NSW, Australia

Abstract The inorganic chlorine (Cl_y) and odd nitrogen (NO_y) chemical families influence stratospheric O_3. In January 2020 Australian wildfires injected record-breaking amounts of smoke into the southern stratosphere. Within 1–2 months ground-based and satellite observations showed Cl_y and NO_y were repartitioned. By May, lower stratospheric HCl columns declined by ~30% and $ClONO_2$ columns increased by 40%–50%. The Cl_y perturbations began and ended near the equinoxes, increased poleward, and peaked at the winter solstice. NO_2 decreased from February to April, consistent with sulfate aerosol reactions, but returned to typical values by June - months before the Cl_y recovery. Transport tracers show that dynamics not chemistry explains most of the observed O_3 decrease after April, with no significant transport earlier. Simulations assuming wildfire smoke behaves identically to sulfate aerosols couldn't reproduce observed Cl_y changes, suggesting they have different composition and chemistry. This undermines our ability to predict ozone in a changing climate.

Plain Language Summary Smoke injected into the stratosphere by the massive 2020 Australian wildfires affected stratospheric chemical composition in a way never before seen. These changes occurred gradually over a 4–5 month period after the fires, then gradually reversed over another 4 months. The greatest changes involved chemicals containing chlorine, which can affect stratospheric ozone amounts. Satellite data showed that lower stratospheric aerosol levels in the southern hemisphere middle latitudes were more than doubled for about 5 months. Model simulations using stratospheric sulfate aerosol reactions were unable to reproduce the observed changes in the chlorine species. This means that the Australian wildfire smoke did not behave chemically like sulfate aerosols. It's important to figure out what chemical reactions occur on wildfire aerosols so we can predict how stratospheric ozone will be impacted if massive wildfires occur more often in a warming climate.

1. Introduction

The discovery of the cause of the Antarctic ozone hole revealed the unanticipated role that heterogeneous chemistry on stratospheric particle surfaces plays on composition. In the cold, dark Antarctic winter stratosphere, these surface reactions convert reactive nitrogen (NO_x) to HNO_3, and HCl and $ClONO_2$ to Cl_2. Returning sunlight initiates catalytic ozone loss via O_3 + Cl (Solomon, 1990). The rapid springtime depletion of Antarctic ozone is now well simulated by models because the reactions on various particle surfaces have been identified and their rates characterized in laboratory studies. Heterogeneous reactions also occur on stratospheric sulfate aerosols outside the polar regions and become important after large injections of volcanic aerosols (Koike et al., 1994; Tie et al., 1994). At midlatitude temperatures (i.e., >200K), the primary impact of volcanic aerosol reactions is conversion of nitrogen oxides ($NO_x = NO + NO_2 + NO_3 + N_2O_5$) to HNO_3 (Hofmann & Solomon, 1989); chlorine repartitioning is minor above 200K. These partitioning changes affect ozone because the NO_x catalytic cycle strongly influences middle stratospheric ozone; in the lower stratosphere (LS), ozone's response also depends on chlorine loading (Tie & Brasseur, 1995). The impact of volcanic sulfate aerosol reactions on ozone and NO_2 is well simulated by models (e.g., Aquila et al., 2013).

Very large pyrocumulonimbus (PyroCb) clouds created by massive wildfires inject tropospheric air and smoke aerosols into the LS, for example, the Canadian Pacific Northwest Event (PNE) in 2017, the Australian Black

Saturday fires in 2009, and the Australian New Year (ANY) fires in 2020 (Schwartz et al., 2020 and references therein). The ANY fires occurred from 29 December 2019 to 7 January 2020 and injected an estimated smoke mass of 0.3–2.1 Tg into the stratosphere (Hirsch & Koren, 2021; Peterson et al., 2021; Torres et al., 2020; Yu et al., 2021). Some material rose as high as ∼32 km due to aerosol self-heating (Kablick et al., 2020; Khaykin et al., 2020). Within a few weeks, satellite measurements of aerosol optical depth and extinction throughout the southern hemisphere (SH) LS were elevated well above background levels; enhanced aerosol levels persisted throughout 2020 (Hirsch & Koren, 2021; Peterson et al., 2021; Rieger et al., 2021; Santee et al., 2022; Solomon et al., 2022; Yu et al., 2021).

The stratospheric chemical reactivity of black and brown carbon aerosols is unknown. Yu et al. (2021) assumed that aging aerosols acquire a sulfate coating, giving them the same reactivity as background stratospheric aerosols; they estimated the ANY stratospheric smoke injection to be 2.5% black carbon and 97.5% organics by mass. Bernath et al. (2022) reported spectral signatures of oxygenated hydrocarbons and adsorbed water in the ANY smoke particles. Murphy et al. (2021) measured composition in stratospheric PNE smoke aerosols and found them to be rich in organics, making them less acidic than typical stratospheric sulfate aerosols. Ditas et al. (2018) used northern hemisphere aircraft observations to estimate that the coating that grows on smoke aerosols in the LS is 30% condensed volatile organic compounds (VOCs) while the remainder may be explained by condensed oxygenated VOCs and sulfate. Some lab studies suggest that organic-rich coatings on smoke aerosols may enhance HCl uptake by sulfate aerosols and reduce hydrolysis of N_2O_5 (Park et al., 2009), which could drive chemistry that differs from sulfuric acid/water (i.e., volcanic) aerosols. However, increased uptake will not change reaction rates unless accompanied by increased solubility (Hanson et al., 1994).

Several studies have reported changes in LS composition, including O_3, resulting from the ANY aerosol and gas injections. Schwartz et al. (2020) reported enhancements of biomass burning products (e.g., CO, HCN, CH_3OH) and water vapor in Microwave Limb Sounder (MLS) satellite data sets up to 4 months following the fires and as high as 5.6 hPa (∼35 km). Solomon et al. (2022) reported depleted LS NO_x in Mar/Apr from satellite data and used model sensitivity tests of N_2O_5 hydrolysis on smoke to estimate that the NO_x suppression reduced column O_3 by ∼1% (∼3 DU) in March. Santee et al. (2022) used MLS and Atmospheric Chemistry Experiment Fourier Transform Spectrometer (ACE) data to show repartitioning between HCl, $ClONO_2$, and ClO that was well outside of the range of nearly 20 years of observations, but found no clear signature of chemical O_3 depletion. Bernath et al. (2022) also used ACE trace gases to show Cl_y repartitioning and argued for O_3 depletion in July. In experiments with the CARMA microphysical model coupled to the Community Earth System Model (CESM-CARMA), Yu et al. (2021) assumed ANY smoke aerosols were sulfate-coated and attributed 5–10 DU ozone depletion to ANY aerosols between August and December 2020, 40–70°S. These studies provide no consensus for the magnitude, timing, or distribution of O_3 depletion.

In this paper we use observations and the Global Modeling Initiative (GMI) chemistry transport model (CTM) to investigate chlorine and nitrogen family repartitioning by sulfate aerosols. Because chemistry and transport both affect LS O_3, we use time series of long-lived trace gases identify the role, timing, and cause of the transport that decreased O_3 during austral fall and winter. Model simulations failed to produce the observed chlorine repartitioning, suggesting an unknown heterogeneous chemical pathway. The inability to simulate the repartitioning of key chemical families controlling stratospheric ozone is significant and could undermine the credibility of ozone projections in a changing climate.

2. Data Sets and Model Simulations

We use a suite of trace gas and aerosol measurements from satellite and ground-based instruments to compare the temporal evolution of LS composition in 2020 to previous years. We also show composition differences in 3 GMI CTM simulations integrated with varying sulfate aerosol surface area densities (SAD) to examine the sensitivity of Cl_y and odd nitrogen (NO_y) partitioning to aerosol loading.

To monitor composition changes, we use total and partial trace gas columns, including HNO_3, HCl, $ClONO_2$, NO_2, N_2O, HF, and O_3 measured by FTIR spectrometer in Lauder, New Zealand (45°S, 170°E). These data sets are part of the Network for the Detection of Atmospheric Composition Change (NDACC, http://www.ndacc.org; De Mazière et al., 2018). All figures show 10-day averages to reduce short-term variability. These data are complemented by MLS v5.0 pressure level measurements of HNO_3, HCl, ClO, temperature and O_3 (Livesey
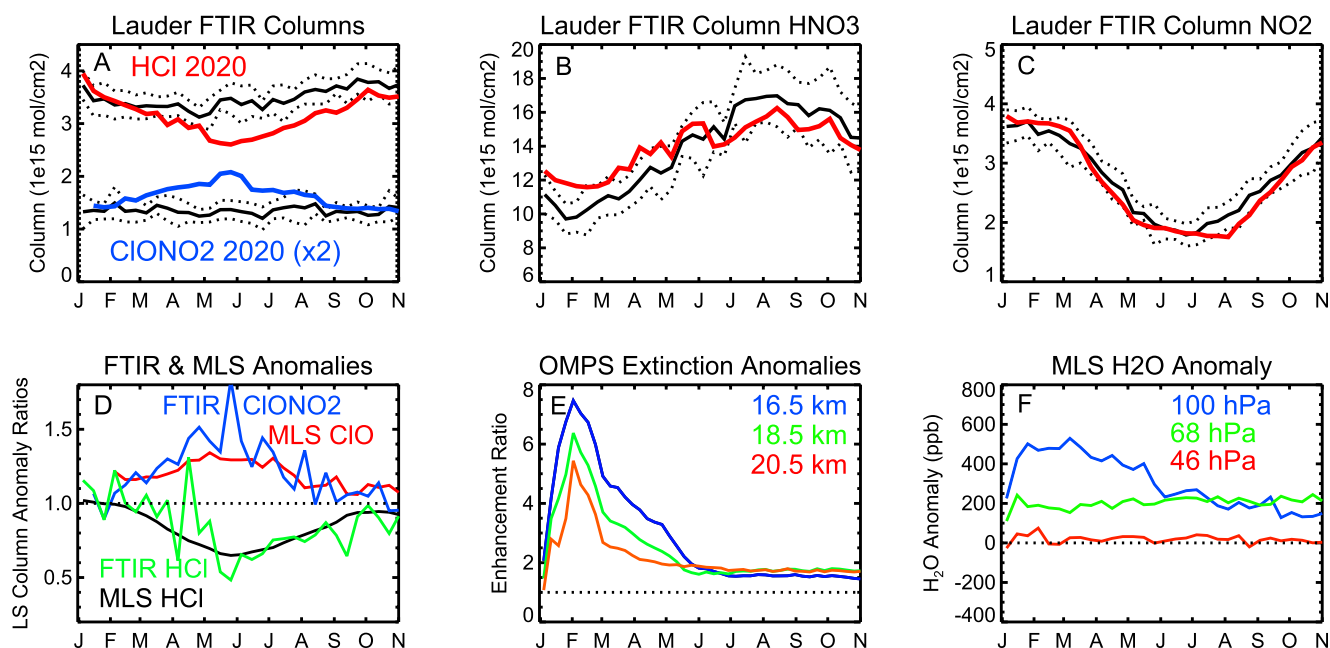
Figure 1. 10-day average Lauder FTIR column measurements in 2020 (color) and their 2010–2019 means (black) and 1 standard deviation (dotted) for (a) HCl and ClONO$_2$ (note scaling), (b) HNO$_3$, and (c) NO$_2$. (d) lower stratosphere (LS) columns (~150–50 hPa, ~12–20 km) of 10-day average 2020 FTIR HCl (green), Microwave Limb Sounder (MLS) HCl (black) and MLS ClO (red), and total column FTIR ClONO$_2$ (blue) ratioed to their 10-year means. There is insufficient signal for a LS ClONO$_2$ column. (e) Weekly-average ZM 2020 Ozone Mapping and Profiler Suite (OMPS) 869 nm extinctions ratioed to their 2013–2019 mean at 3 altitudes. (f) 10-day average MLS ZM H$_2$O anomalies (ppb) relative to the 2010–2019 mean at 3 pressure levels comparable to the OMPS altitudes. All satellite data are averaged 40–50°S.

et al., 2021) and by ACE satellite v4.1 sunset data for ClONO$_2$, HCl, HNO$_3$, and NO$_2$ (Boone, Bernath, Cok, et al., 2020). All MLS data are shown as zonal means (ZM). The Ozone Mapping and Profiler Suite (OMPS) Limb Profiler instrument provides high vertical resolution (1 km) aerosol extinction profiles in the 510–1,000 nm spectral range (Taha et al., 2021).

To test whether sulfate aerosol chemistry alone suffices to explain the observations, we ran three simulations of the GMI CTM (Strahan et al., 2013) that differ only in SAD amounts. Simulations were integrated with Modern-Era Retrospective Analysis for Research and Applications 2 (MERRA2) meteorology at 1° × 1.25° horizontal resolution on 72 hybrid sigma-pressure levels (Gelaro et al., 2017). The GMI stratospheric heterogeneous chemistry includes reactions with HNO$_3$, HCl, H$_2$O, ClONO$_2$, and BrONO$_2$ on sulfate aerosols, saturated ternary solutions, nitric acid trihydrate, and ice particles (e.g., Solomon et al., 2015). Only the sulfate aerosols have nonzero surface area outside of the polar low temperature regions; their reactions are listed in the Supporting Information S1. The "'Baseline" simulation, integrated from 1980 to 2020, uses observationally-derived monthly ZM stratospheric sulfate SADs for 2000–2018. SADs averaged over 2009–2018 were used for 2019 and 2020. We simulated the effects of ANY aerosols by estimating sulfate aerosol SAD fields from the monthly mean latitude and height distributions of 2020 OMPS 869 nm extinctions. The mapping between extinction and SAD amount was derived from the relationship between OMPS extinctions and the SAD fields for the overlapping years, 2013–2018. This estimate of the 2020 SAD fields was used in a 1-year GMI CTM simulation "OMPS-SAD." We further tested the sensitivity to SADs in a simulation where the OMPS-derived SAD fields were increased fivefold ("OMPS-SAD5").

3. Observations of Aerosol Extinction, Chlorine and Nitrogen Species

Total columns of nitrogen and chlorine trace gases measured at Lauder (45°S) illustrate remarkable changes in some species, while others lie within the range of past observations (Figure 1). The column HCl abundance in early 2020 was similar to previous years but dropped below the mean from late February until late May, when it sank well below all measurements in the previous decade. It increased from June to October, when it returned to

within 1 standard deviation (σ) of the mean. Like a mirror image, the FTIR $ClONO_2$ column abundance exceeded the mean by more than 50% in late May, then declined to typical values in September. Large opposing HCl and $ClONO_2$ perturbations were also measured by FTIR at Wollongong (34°S) and Arrival Heights (78°S); see Figure S1 in Supporting Information S1. The large April anomalies at Arrival Heights indicate that smoke reached the Antarctic region prior to vortex formation. Notice that in late May, the Lauder HCl column decline is twice that of the $ClONO_2$ increase, suggesting at face value that Cl_y isn't conserved. Global Modeling Initiative simulations show that HCl and $ClONO_2$ constitute ~97% of the midlatitude Cl_y column, 70%–80% of which resides in the LS. Observed column HNO_3 and NO_2 deviations from climatology never exceeded ~1σ (Figures 1b and 1c).

Figure 1d shows that the $ClONO_2$ column changes are paralleled by changes in the MLS LS ClO column (40–50°S), with both species having similar large enhancements in early June. Excellent agreement is seen between the MLS LS HCl (40–50°S) and the FTIR LS column reductions, both declining 30% by 1 June. By October Cl_y partitioning is within the range of previous years. Similar findings were reported by Santee et al. (2022) and Bernath et al. (2022).

OMPS 869 nm extinction enhancements between 16 and 20 km (~100–50 hPa) and 40–50°S rose rapidly in January at the time of the wildfires, peaked near 1 February, then rapidly decayed for a month (Figure 1e). In March the extinction enhancement decay rate abruptly slowed, coinciding with the onset of the Cl_y anomalies. (Elevated ClO in early February may indicate continued interference from elevated CH_3OH (Santee et al., 2022; Schwartz et al., 2020)). The decay rate slowed further in June when the Cl_y anomalies reached their maximum. The aerosol extinction decay rate (Figure S2 in Supporting Information S1) has the same shape as the enhancement decay rate (Figure 1e). Lauder lidar extinction measurements at 532 nm were also enhanced in the LS throughout 2020 (Figure S3 in Supporting Information S1). Santee et al. (2022) suggest that the enhancements in MLS 100 hPa water vapor (Figure 1f) may be attributable to the wet phase of the tropical tape recorder. They showed that 2020 MLS SH midlatitude LS water (~4 ppm) and MERRA2 temperature (212–224 K) were within the 2005–2019 data envelope. These conditions are warmer and drier than the cold moist conditions above thunderstorms penetrating the tropopause that have been proposed to cause significant water-enhanced O_3 depletion via NO_x reduction and ClO enhancement (Anderson et al., 2012).

ACE profile anomalies in Figure 2 indicate that the mirrored changes in HCl and $ClONO_2$ columns (Figure 1) have mirrored changes in their vertical distributions. Figures 2a and 2b show ACE HCl and $ClONO_2$ LS anomaly development (40–50°S) from February to August. Mirrored anomalies of 0.4–0.5 ppb develop between February and June, peaking at 50–60 hPa. This alters chlorine reservoir gas mixing ratios by up to −50% for HCl and +100% for $ClONO_2$; see Figure S4 in Supporting Information S1 for ACE profiles. The August anomalies show a significant reversal from June, consistent with the findings of Santee et al. (2022).

The clearest indication of NO_y repartitioning is shown by changes in the ACE NO_2 anomaly profile between February and Apr (Figure 2c). It is near zero in February but strongly negative by April; the April data are lower than all other April ACE means (see Figure S5 in Supporting Information S1). Similarly, Lauder column NO_2 measurements (Figure 1c) are slightly above the decadal mean from January–March but dip below the mean in April and May, returning to the mean in June. Solomon et al. (2022) show very low SH midlatitude NO_2 at 18.5 km 30–60°S measured by satellite instruments in February and March 2020 with greater sampling than ACE or the Lauder FTIR. The combined data sets indicate LS NO_2 suppression consistent with hydrolysis of N_2O_5 ($N_2O_5 + H_2O \rightarrow 2\ HNO_3$) on sulfate aerosols from February to April. After April the repartitioning reverses and is again near zero in June. It is curious that the aerosols' NO_2 impact appears to end by June while their Cl_y impact persisted for several months longer.

Interannual transport variations in fall and winter cause long-lived trace gases such as HCl and HNO_3 to vary by up to ~10% compared to their decadal means. This corresponds to variations in MLS HNO_3 of ±0.5 ppb on the 46 and 68 hPa levels (Figure S6 in Supporting Information S1). The aerosol-driven changes in NO_2 in Figure 2c are −0.2 ppb or less, thus a corresponding +0.2 ppb increase in LS HNO_3 would not be distinguishable from transport-driven variations. The ACE April LS NO_2 anomalies represent record low mixing ratios that are 25%–30% below the decadal mean (Figure S5 in Supporting Information S1), suggesting significant repartitioning. Santee et al. (2022) used HCl/N_2O correlations to demonstrate that transport could not explain the chlorine repartitioning.
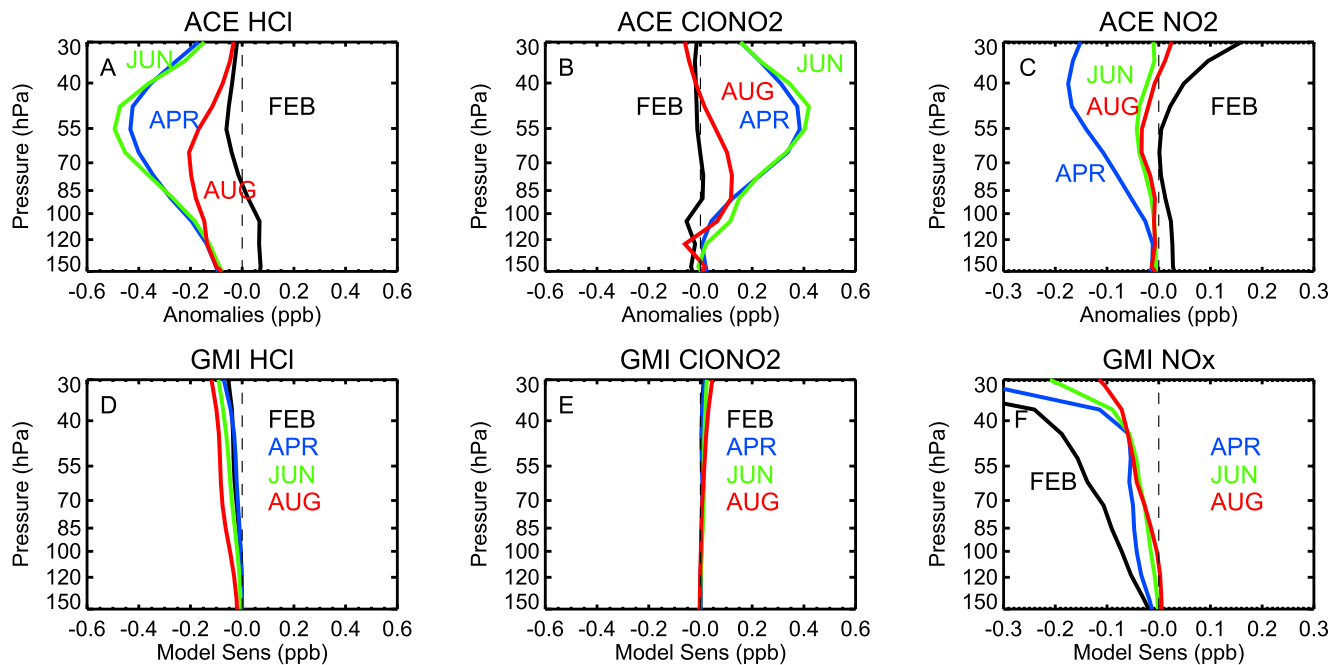
Figure 2. ACE monthly ZM 40–50°S anomalies (ppb) relative to 2010–2019 means for (a) HCl, (b) ClONO$_2$ and (c) NO$_2$. Monthly ZM 40–50°S Global Modeling Initiative (GMI) sensitivities relative to Baseline for (d) HCl (Ozone Mapping and Profiler Suite(OMPS)-SAD5), (e) ClONO$_2$ (OMPS-SAD5), and (f) NO$_x$ (OMPS-SAD). Simulated lower stratosphere (LS) NO$_x \approx 2 \times$ NO$_2$.

4. Simulated Repartitioning

The magnitude and timing of the observed Cl$_y$ repartitioning are inconsistent with the simulated sulfate aerosol chemistry. The differences between HCl and ClONO$_2$ profiles from the OMPS-SAD5 and the Baseline simulations indicate very little sensitivity to enhanced SADs (Figures 2d and 2e); Cl$_y$ results from the OMPS-SAD simulation (not shown) have near zero difference from the Baseline. The simulated sensitivity increases with height, unlike the observations which have a maximum near 50 hPa, and the HCl reduction is much greater than the ClONO$_2$ increase (i.e., no mirroring). Increased simulated ClO$_x$ balances the HCl reduction (not shown). Simply boosting the OMPS-derived SAD levels fivefold did not improve agreement with observations.

While the OMPS-SAD run suppresses LS NO$_x$ (Figure 2f), unlike observations it does so immediately after the aerosol injection and is recovering by April. In contrast, the observed ACE NO$_2$ anomaly is near zero in February and reaches its maximum in April. NO$_x$ suppression in the OMPS-SAD5 simulation (not shown) is much larger and persists too long, increasing the disagreement with observations.

In contrast to the observations, the simulated Cl$_y$ and NO$_y$ repartitioning begins immediately after the aerosol injections and changes in the chemical species have different magnitudes, durations, and vertical distributions. The model's inability to reproduce these effects indicates ANY aerosol reactivity differs in some ways from that of volcanic sulfate aerosols.

5. The Pattern of Cl$_y$ Repartitioning

Figure 3 shows the temporal and spatial evolution of the midlatitude MLS HCl reduction, MLS temperature, and OMPS extinction enhancement near 18 km where the peak HCl anomaly occurs. HCl reductions distinguishable from transport variability (i.e., greater than 10%) are found from ~25 to 60°S, from March until October, and increase with increasing latitude. The HCl anomaly pattern shows no clear relationship to temperature (Figure 3b); for example, the HCl anomaly maximum 55–60°S occurs about 1.5 months before the temperature minimum. The HCl anomalies begin about a month after the peak extinction enhancements, suggesting the importance of aerosol aging to initiation of heterogeneous reactions. Notice that the lower latitudes, where aerosol enhancement is greater and temperatures are lower, have the smallest HCl reductions.
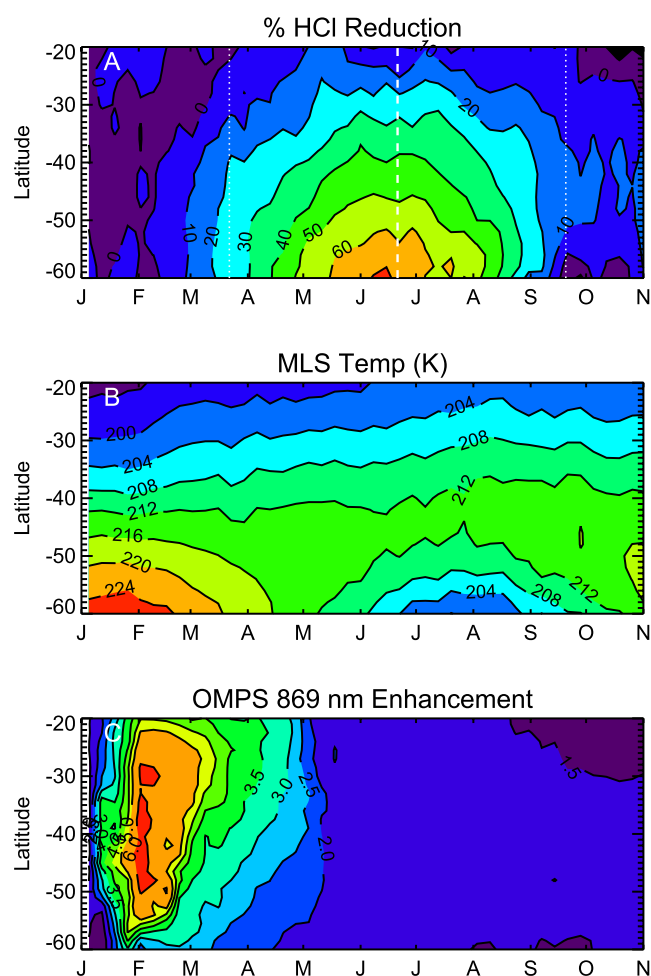
Figure 3. (a) 2020 weekly ZM percent reduction in Microwave Limb Sounder (MLS) HCl (68 hPa) relative to 2010–2019 mean. Polar processing may contribute to reductions near 60°S. White lines indicate solstice and equinoxes. Weekly ZM (b) MLS temperature (68 hPa) and (c) Ozone Mapping and Profiler Suite (OMPS) 869 nm extinction enhancement at 18.5 km relative to the 2013–2019 mean.

Reduced sunlight appears important to the development and persistence of the anomalies: the HCl reduction shows symmetry about its maximum at the winter solstice (dashed line), it begins and ends near the equinoxes (dotted lines) and does not follow temperature changes. The anomalies decrease with decreasing latitude as sunlight increases. Both the NDACC and MLS data (Figure S1 in Supporting Information S1 and Figure 3a) show that Cl_y repartitioning at 34°S (Wollongong) ended 1 month earlier and HCl is less reduced than at 45°S (Lauder), consistent with a dependence on sunlight. The OMPS-SAD5 simulation's HCl reduction, shown in Figure S7 of Supporting Information S1, is far smaller than the observations, it does not show solstice symmetry, and it increases where temperatures are lowest. Santee et al. (2022) reported that no previous HCl perturbation of this scale exists in the MLS record.

Conditions in 2020 were too warm and dry for significant NO_x reduction and ClO enhancement through standard sulfate aerosol chemistry. It is likely that the wildfire aerosols were responsible and that their composition allowed unidentified heterogeneous chemical reactions. With aerosol enhancements below a factor of 2 after mid-May, gas phase photochemistry may control the anomaly reversal from June to October.

6. Ozone Changes and the Role of Transport

Cl_y and NO_y partitioning impacts ozone chemistry (Solomon et al., 1996; Tie & Brasseur, 1995; Tie et al., 1994). LS O_3 columns measured by Lauder FTIR and by MLS were slightly above their respective 10-year climatologies from January–April (Figures 4a and 4b), but from May to October each was $\sim 1\sigma$ below their means, representing a ~ 10 DU drop in the ~ 150–50 hPa layer (8%–10%). LS O_3 is long-lived and transport plays a dominant role in its distribution. Transport must be accounted for before O_3 depletion can be identified or quantified.

LS columns of the long-lived tracers HF and N_2O, and total column Cl_y (HCl + $ClONO_2$) provide excellent transport information (Figures 4d–4f). Because Cl_y, HF, and O_3 mixing ratios increase with altitude (and latitude) while N_2O decreases, the N_2O response to transport opposes the other species. All tracers have columns near climatology from January–April but shift in unison in early May. The simultaneous increase in N_2O and decreases in Cl_y and HF indicate that transport caused the air to become younger starting in May. Younger air has lower Cl_y, which explains the apparent lack of conservation between column HCl and $ClONO_2$ changes in late May (Figure 1a). These species' 2020 anomalies, including O_3, all tell the same tale in Figure 4: the midlatitude LS became persistently younger in May. Note that the tracers are scaled differently because of their widely different atmospheric abundances. Bernath et al. (2022) attributed low O_3 45–60°S in July 2020 to the ANY fires but did not consider transport effects. We estimate the negative LS O_3 anomaly in their Figure 2 equals ~ 6 DU, an amount smaller than the 10–15 DU LS column O_3 changes we attribute to transport that began in May (Figures 4a and 4b). While some depletion probably occurred due to elevated ClO, the large transport-driven changes that occurred mid-year make quantifying a small loss difficult.

The younger air in 2020 is explained by the Quasi Biennial Oscillation's (QBO) meridional circulation that develops as the Brewer Dobson Circulation strengthens in austral fall. The QBO was in the easterly phase below 30 hPa in the austral fall and winter 2020, which increased the quasi-horizontal transport of young tropical air to the midlatitudes (Strahan et al., 2015).
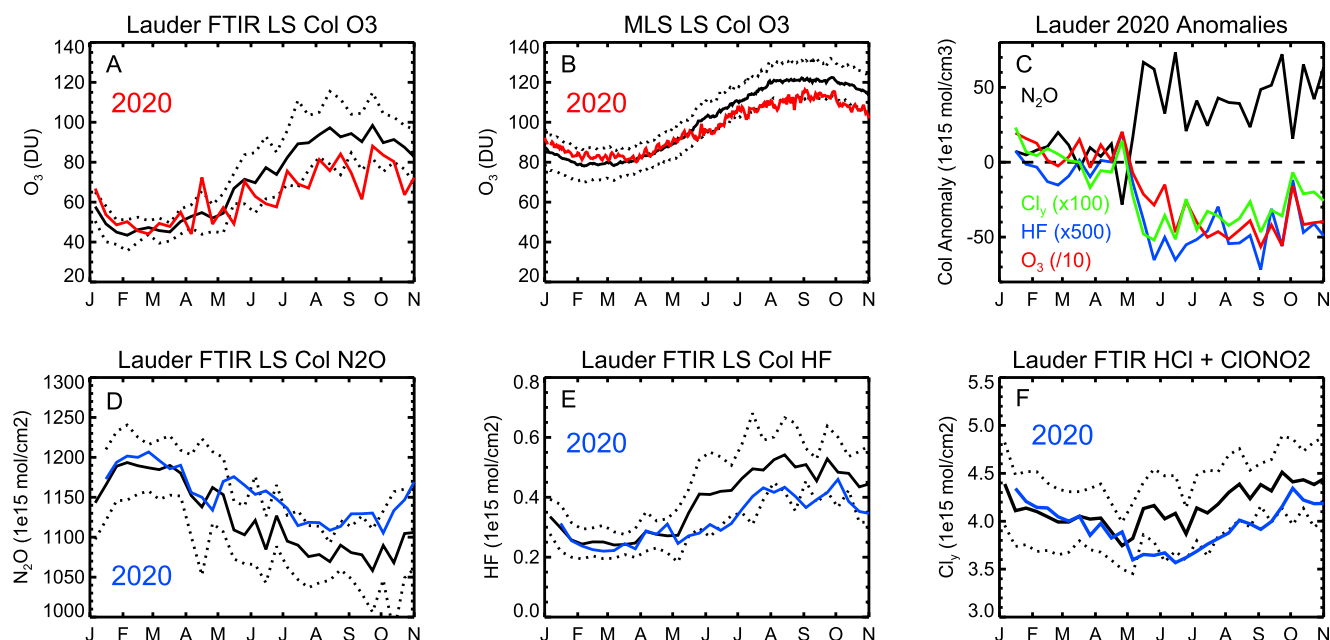
Figure 4. 2020 trace gas columns compared to the 2010–2019 mean and 1σ (a) Lauder FTIR lower stratosphere (LS) O_3, (b) Microwave Limb Sounder (MLS) ZM LS O_3 (46°S). (c) 2020 column anomalies for data shown in panels a, d, e, and f (scaled); FTIR (d) LS N_2O, (e) LS HF, and (f) total column $HCl + ClONO_2$ ($\approx Cl_y$).

7. Conclusions

Ground-based column data combined with data from three satellite instruments show that 1–2 months after the ANY fires, midlatitude Cl_y was conserved but significantly repartitioned from March to September 2020. It is likely that Cl_y and NO_y repartitioning occurred via heterogeneous chemical reactions on the wildfire aerosols. We found that the Cl_y repartitioning occurred symmetrically about the austral winter solstice, beginning and ending near the equinoxes. These temporal clues and the poleward increase in the anomaly magnitude suggest that reduced sunlight is essential for creating and maintaining the repartitioned state. The timing of the anomaly onset suggests the importance of aerosol aging to initiation of heterogeneous reactions. Changes in long-lived trace gases N_2O, HF, and Cl_y made it clear that the ∼10 DU O_3 decrease after April was driven largely by transport that began in May. Elevated MLS ClO implies some O_3 loss occurred. Unlike Antarctic conditions, the presence of elevated $ClONO_2$ throughout the midlatitudes indicates a deactivation pathway for ClO that limits depletion.

None of the enhanced SAD simulations of the GMI CTM produced Cl_y repartitioning that resembled the observations, indicating that the ANY aerosol chemistry differs from that of volcanic sulfate aerosols. The enhanced SAD simulations suppressed NO_2 but the timing and duration differed from the ACE observations. Schwartz et al. (2020) report enhanced stratospheric CH_3OH and other biomass burning products in the first few months after the fires. Observational studies measuring stratospheric particle composition, volatile organic and oxygenated organic species (Bernath et al., 2022; Boone, Bernath, & Fromm, 2020; Ditas et al., 2018; Murphy et al., 2021) showed that aged smoke aerosols carry high levels of oxygenated organics in their coatings, rendering them less acidic than sulfate aerosols. These composition changes are likely to alter heterogeneous reaction rates that impact Cl_y and NO_y species. This may explain our inability to simulate the observed repartitioning using reactions and rates appropriate for volcanic sulfate aerosols. Laboratory studies to identify the reactions occurring on lower acidity, organic-rich sulfate aerosols are urgently needed.

PyroCbs were a newly identified phenomenon only 2 decades ago but recently they have become more frequent as climate change causes soils to dry out due to extreme temperatures, droughts to persist and expand their range, and large forest fires to ignite earlier in summer, lengthening the fire season (Canadell et al., 2021; Peterson et al., 2021). It is very likely that the ANY aerosols repartitioned the Cl_y and NO_y families, whose radical members react with O_3. The 2020 observations shown here and in other studies and our inability to simulate them have revealed a gap in our understanding of the key processes controlling stratospheric O_3. This knowledge gap weakens the credibility of the chemistry climate models we use to project future O_3 levels.

Conflict of Interest

The authors declare no conflicts of interest relevant to this study.

Data Availability Statement

References

Anderson, J. G., Wilmouth, D. M., Smith, J. B., & Sayres, D. S. (2012). UV dosage levels in summer: Increased risk of ozone loss from convectively injected water vapor. *Science*, *337*(6096), 835–839. https://doi.org/10.1126/science.1222978

Aquila, V., Oman, L. D., Stolarski, R., Douglass, A. R., & Newman, P. A. (2013). The response of ozone and nitrogen dioxide to the eruption of Mt. Pinatubo at southern and northern midlatitudes. *Journal of the Atmospheric Sciences*, *70*(3), 894–900. https://doi.org/10.1175/jas-d-12-0143.1

Bernath, P., Boone, C., & Crouse, J. (2022). Wildfire smoke destroys stratospheric ozone. *Science*, *375*(6586), 1292–1295. https://doi.org/10.1126/science.abm5611

Boone, C. D., Bernath, P. F., Cok, D., Jones, S. C., & Steffen, J. (2020). Version 4 retrievals for the atmospheric chemistry experiment Fourier transform spectrometer (ACE-FTS) and imagers. *Journal of Quantitative Spectroscopy and Radiative Transfer*, *247*, 106939. https://doi.org/10.1016/j.jqsrt.2020.106939

Boone, C. D., Bernath, P. F., & Fromm, M. D. (2020). Pyrocumulonimbus stratospheric plume injections measured by the ACE-FTS. *Geophysical Research Letters*, *47*(15), e2020GL088442. https://doi.org/10.1029/2020GL088442

Canadell, J. F., Meyer, C. P., Cook, G. D., Dowdy, A., Briggs, P. R., Knauer, J., et al. (2021). Multi-decadal increase of forest burned area in Australia is linked to climate change. *Nature Communications*, *12*(1), 6921. https://doi.org/10.1038/s41467-021-27225-4

De Mazière, M., Thompson, A. M., Kurylo, M. J., Wild, J. D., Bernhard, G., Blumenstock, T., et al. (2018). The network for the detection of atmospheric composition change (NDACC): History, status and perspectives. *Atmospheric Chemistry and Physics*, *18*(7), 4935–4964. https://doi.org/10.5194/acp-18-4935-2018

Ditas, J., Ma, N., Zhang, Y., Assmann, D., Neumaier, M., Riede, H., et al. (2018). Strong impact of wildfires on the abundance and aging of black carbon in the lowermost stratosphere. *Proceedings of the National Academy of Sciences*, *115*(50), E11595–E11603. https://doi.org/10.1073/pnas.1806868115

Gelaro, R., McCarty, W., Suarez, M. J., Todling, R., Molod, A., Takacs, L., et al. (2017). The modern-era retrospective analysis for research and applications, version 2 (MERRA-2). *Journal of Climate*, *30*(14), 5419–5454. https://doi.org/10.1175/jcli-d-16-0758.1

Hanson, D. R., Ravishankara, A. R., & Solomon, S. (1994). Heterogeneous reactions in sulfuric acid aerosols: A framework for model calculations. *Journal of Geophysical Research*, *99*(D2), 3615–3629. https://doi.org/10.1029/93jd02932

Hirsch, E., & Koren, I. (2021). Record-breaking aerosol levels explained by smoke injection into the stratosphere. *Science*, *371*(6535), 1269–1274. https://doi.org/10.1126/science.abe1415

Hofmann, D. J., & Solomon, S. (1989). Ozone destruction through heterogeneous chemistry following the eruption of El Chichon. *Journal of Geophysical Research*, *94*(D4), 5029–5041. https://doi.org/10.1029/jd094id04p05029

Kablick, G. P., III, Allen, D. R., Fromm, M. D., & Nedoluha, G. E. (2020). Australian pyroCb smoke generates synoptic-scale stratospheric anticyclones. *Geophysical Research Letters*, *47*(13), e2020GL088101. https://doi.org/10.1029/2020GL088101

Khaykin, S., Legras, B., Bucci, S., Sellitto, P., Isaksen, L., Tence, F., et al. (2020). The 2019/20 Australian wildfires generated a persistent smoke-charged vortex rising up to 35 km altitude. *National Communications Earth & Environment*, *1*(22). https://doi.org/10.1038/s43247-020-00022-5

Koike, M., Jones, N. B., Matthews, W. A., Johnston, P. V., McKenzie, R. L., Kinnison, D., & Rodriguez, J. M. (1994). Impact of Pinatubo aerosols on the partitioning between NO_2 and HNO_3. *Geophysical Research Letters*, *21*(7), 597–600. https://doi.org/10.1029/94gl00303

Livesey, N., Read, W. G., Wagner, P. A., Froidevaux, L., Santee, M. L., Schwartz, M. J., et al. (2021). *Earth observing System (EOS) aura Microwave Limb sounder (MLS) version 5.0x level 2 and 3 data quality and description document*. JPL D-105336 Rev A.

Murphy, D. M., Froyd, K. D., Bourgeois, I., Brock, C. A., Kupc, A., Peischl, J., et al. (2021). Radiative and chemical implications of the size and composition of aerosol particles in the existing or modified global stratosphere. *Atmospheric Chemistry and Physics*, *21*(11), 8915–8932. https://doi.org/10.5194/acp-21-8915-2021

Park, S.-C., Burden, D. K., & Nathanson, G. M. (2009). Surfactant control of gas transport and reactions at the surface of sulfuric acid. *Accounts of Chemical Research*, *42*(2), 379–387. https://doi.org/10.1021/ar800172m

Peterson, D. A., Fromm, M. D., McRae, R. H. D., Campbell, J. R., Hyer, E. J., Taha, G., et al. (2021). Australia's Black Summer pyrocumulonimbus super outbreak r-eveals potential for increasingly extreme stratospheric smoke events. *NPJ climate and atmospheric science*, *4*(38). https://doi.org/10.1038/s41612-021-00192-9

Rieger, L. A., Randel, W. J., Bourassa, A. E., & Solomon, S. (2021). Stratospheric temperature and ozone anomalies associated with the 2020 Australian bushfires. *Geophysical Research Letters*, *48*(24), e2021GL095898. https://doi.org/10.1029/2021GL0958989

Santee, M. L., Lambert, A., Manney, G. L., Livesey, N. J., Froidevaux, L., Neu, J., et al. (2022). Prolonged and pervasive perturbations in the composition of the southern hemisphere midlatitude lower stratosphere from the Australian New Year's Fires. *Geophysical Research Letters*, *49*(4). https://doi.org/10.1029/2021GL096270

Schwartz, M. J., Santee, M. L., Pumphrey, H. C., Manney, G. L., Lambert, A., Livesey, N. J., et al. (2020). Australian new year's pyroCb impact on stratospheric composition. *Geophysical Research Letters*, *47*(24), e2020GL090831. https://doi.org/10.1029/2020GL090831

Solomon, S. (1990). Progress toward a quantitative understanding of Antarctic ozone depletion. *Nature*, *347*(6291), 347–354. https://doi.org/10.1038/347347a0

Solomon, S., Dube, K., Stone, K., Yu, P., Kinnison, D., Toon, O. B., et al. (2022). On the stratospheric chemistry of mid-latitude wildfire smoke. *Proceedings of the National Academy of Sciences*, *119*(10), e2117325119. https://doi.org/10.1073/pnas.2117325119

Solomon, S., Kinnison, D., Bandoro, J., & Garcia, R. (2015). Simulation of polar ozone depletion: An update. *Journal of Geophysical Research: Atmospheres*, *120*(15), 7958–7974. https://doi.org/10.1002/2015JD023365

Solomon, S., Portmann, R. W., Garcia, R. R., Thomason, L. W., Poole, L. R., & McCormick, M. P. (1996). The role of aerosol variations in anthropogenic ozone depletion at northern midlatitudes. *Journal of Geophysical Research*, *101*(D3), 6713–6727. https://doi.org/10.1029/95jd03353

Strahan, S. E., Douglass, A. R., & Newman, P. A. (2013). The contributions of chemistry and transport to low Arctic ozone in March 2011 derived from Aura MLS Observations. *Journal of Geophysical Research: Atmospheres*, *118*(3), 1563–1576. https://doi.org/10.1002/jgrd.50181

Strahan, S. E., Oman, L. D., Douglass, A. R., & Coy, L. (2015). Modulation of Antarctic vortex composition by the quasi-biennial oscillation. *Geophysical Research Letters*, *42*(10), 1–8. https://doi.org/10.1002/2015gl063759

Taha, G., Loughmann, R., Zhu, T., Thomason, L., Kar, J., Rieger, L., & Bourassa, A. (2021). OMPS LP Version 2.0 multi-wavelength aerosol extinction coefficient retrieval algorithm. *Atmospheric Measurement Techniques*, *14*(2), 1015–1036. https://doi.org/10.5194/amt-14-1015-2021

Tie, X. X., & Brasseur, G. P. (1995). The response of stratospheric ozone to volcanic eruptions: Sensitivity to atmospheric chlorine loading. *Geophysical Research Letters*, *22*, 3035–3038. https://doi.org/10.1029/95gl03057

Tie, X. X., Brasseur, G. P., Briegleb, B., & Granier, C. (1994). Two-dimensional simulation of Pinatubo aerosol and its effect on stratospheric ozone. *Journal of Geophysical Research*, *99*(D10), 20545–20562. https://doi.org/10.1029/94jd01488

Torres, O., Jethva, H., Ahn, C., Jaross, G., & Loyola, D. G. (2020). TROPOMI aerosol products: Evaluation and observations of synoptic-scale carbonaceous aerosol plumes during 2018–2020. *Atmospheric Measurement Techniques*, *13*(12), 6789–6806. https://doi.org/10.5194/amt-13-6789-2020

Yu, P., Davis, S. M., Toon, O. B., Portmann, R. W., Bardeen, C. G., Barnes, J. E., et al. (2021). Persistent stratospheric warming due to 2019–2020 Australian wildfire smoke. *Geophysical Research Letters*, *48*(7), e2021GL092609. https://doi.org/10.1029/2021GL0926092021

References From the Supporting Information

Burkholder, J. B., Sander, S. P., Abbatt, J., Barker, J. R., Huie, R. E., Kolb, C. E., et al. (2015). *Chemical kinetics and photochemical data for use in atmospheric studies, evaluation No. 18*. JPL Publication. Retrieved from http://jpldataeval.jpl.nasa.gov

Hase, F., Blumenstock, T., & Paton-Walsh, C. (1999). Analysis of the instrumental line shape of high-resolution Fourier transform IR spectrometers with gas cell measurements and new retrieval software. *Applied Optics*, *38*(15), 3417–3422. https://doi.org/10.1364/AO.38.003417

Pougatchev, N. S., Connor, B. J., & Rinsland, C. P. (1995). Infrared measurements of the ozone vertical distribution above Kitt Peak. *Journal of Geophysical Research*, *100*(D8), 16689–16697. https://doi.org/10.1029/95jd01296

Sakai, T., Uchino, O., Nagai, T., Liley, B., Morino, I., & Fujimoto, T. (2016). Long-term variation of stratospheric aerosols observed with lidars over Tsukuba, Japan from 1982 and Lauder, New Zealand from 1992 to 2015. *Journal of Geophysical Research: Atmospheres*, *121*(17), 10283–10293. https://doi.org/10.1002/2016JD025132